

Uniform error bounds for fast calculation of approximate Voigt profiles

Sven Nordebo*,

*Department of Physics and Electrical Engineering, Linnæus University, 351 95 Växjö, Sweden. E-mail: sven.nordebo@lnu.se

Abstract—The broadband line-by-line analysis of radiative transfer in the atmosphere is extremely demanding with regard to computational resources. As a remedy, we present here the calculation of uniform error bounds for approximating the classical Voigt profile. A new “full” Voigt profile, which can be expressed as a combination of two Faddeeva evaluations, is also presented and included in the analysis. The uniform bounds can be used to rigorously determine the domains on which the Voigt profiles can be approximated by the corresponding Lorentz profiles to any desired accuracy. The bounds can furthermore be employed to make a fast and efficient estimate of the most significant lines to be included in a subband adaptive line selection strategy. By using a realistic numerical example of radiative transfer in the atmosphere, we demonstrate that these approximation approaches are able to reduce the computational time of the associated line-by-line analysis by several orders of magnitude with little loss of accuracy.

Index Terms—Radiative transfer in the atmosphere, spectral line shapes, Voigt function, uniform approximation.

I. INTRODUCTION

Even though there are advanced theories of molecular line shapes taking line mixing and velocity changes into account [1], [2], [3], [4], [5], [6], [7], most databases and radiative transfer codes are still using the classical Voigt profile, see *e.g.*, [8], [9], [10], [11]. A simple explanation for this is probably the fact that the broadband line-by-line analysis of radiative transfer in the atmosphere is extremely demanding with regard to computational resources. Quoting Liou [12, p. 126]: “The computer time required for line-by-line calculations, even with the availability of a supercomputer, is formidable. This is especially true for flux calculations in which an integration over all absorption bands is necessary.” Typically, hundreds of thousands of spectral lines must be resolved to a resolution corresponding to millions of frequency points at each atmospheric level. And at the same time, most of these calculations could have been performed based on the simple Lorentzian profile rather than by using the more complex Voigt profile, and most of the spectral line contributions could have been disregarded with very little impact on the final accuracy of the computation. Much of these problems have been overcome with recent line-by-line algorithms based on simplifications, approximations and pre-computed line data, see *e.g.*, [8]. As an aid in the future development, improvement and extension of similar algorithms, this paper is providing rigorous bounds for approximating the Voigt profile by the much simpler Lorentz profile.

The Voigt profile is the convolution between the Lorentzian profile and the Gaussian. And even though there exists computer codes for efficient calculation of the associated Faddeeva function, see *e.g.*, [13], [14], [15], [11], it is much faster just to compute the corresponding Lorentz profile. Moreover, the superexponential Gaussian profile is a highly localized function, a property that can be exploited to significantly accelerate the calculation of an approximate Voigt profile. In this paper we formulate and prove a theorem which quantifies the fact that the Voigt profile converges uniformly towards the Lorentzian profile in two different regards: (1) with respect to the Lorentzian half-width normalized by the Gaussian half-width, and where the approximation error is measured over the whole frequency axis, and (2) with respect to the line width normalized by the Gaussian half-width, and beyond which the far wing approximation error is measured. Thus, (1) if the Lorentzian is sufficiently broad in comparison to the Gaussian, it approximates the Voigt profile everywhere. And (2) in the far wings, the Voigt profile can always be approximated by the Lorentzian, provided that the beginning of the far wing is suitably defined. In this paper we will show how the Voigt (or Faddeeva) function can be used to precalculate the associated threshold values in order to achieve any desired approximation accuracy. The related computations based on thresholding and sorting can readily and efficiently be implemented in a computer code. In a typical application of radiative transfer in the atmosphere, most of the frequency points to be evaluated will fall into the category where these approximations are applicable, and hence the potential to save computation time is almost the same as replacing the Voigt computation for the Lorentzian.

However, the line-by-line computation of broadband radiative transfer in the atmosphere is still huge. To further reduce the computational complexity, a subband (or block) adaptive line selection procedure is presented here. For each spectral line exterior to a fixed and relatively narrow subband, the new error bounds can be used to determine precisely where the Lorentz approximation is applicable, and then very fast and effectively estimate its in-band contribution to any desired accuracy. Thus, the “exterior” spectral lines that are estimated to have a negligible in-band contribution can be excluded from the computation. In-band lines are always included, and the computation can then proceed with the next subband. Even though this is a suboptimal approach, it is a simple, pragmatic and very effective way to include only the lines

that are the most significant, and the procedure can be tuned with very few threshold parameters to control the accuracy. By using realistic numerical examples of radiative transfer in the atmosphere, we will demonstrate that the combination of the two approximation approaches described above can reduce the computational time of the line-by-line analysis by several orders of magnitude with very little loss of accuracy.

In this work we do not attempt to compare the performance of our algorithm with other highly sophisticated commercial codes for radiative transfer such as the MODTRAN 6 line-by-line algorithm reported in [8]. However, a few general remarks can be made as follows. First, the purpose of our numerical example has been to evaluate and compare the proposed approximation methods by using an algorithm that is as simple and straightforward and possible. A layer-recursive algorithm for radiative transfer in a one-dimensional plane-parallel and non-scattering atmosphere has therefore been developed for this purpose. The frequency resolution has been chosen based on the (frequency dependent) Doppler broadening in the upper atmosphere at 65 km height, and is therefore extremely dense with a resolution starting at $75 \cdot 10^{-6} \text{ cm}^{-1}$ in the lower 100 cm^{-1} band. All profiles are calculated on-the-fly, based on line parameters that have been retrieved from the HITRAN database [9], [10]. Similar as with the MODTRAN algorithm, our algorithm is computing Voigt profiles with their line centers within certain narrow subbands. The main difference is the way in which the exterior tail contributions are selected and computed. Our algorithm is employing the adaptive line selection procedure as described above, whereas the MODTRAN algorithm is employing a fixed 25 cm^{-1} maximal distance for their line selection [8, p. 544–545]. The MODTRAN algorithm is furthermore employing pre-computed line shape data which is stored on a fine temperature and coarse pressure grid, and which can then readily be scaled for the adequate pressure on-the-fly. The latter procedure, which is based on Padé approximations of Voigt sums, is no doubt an effective way of making the algorithm very fast.

We will also introduce and incorporate in the analysis the “full” Voigt profile. The full Voigt profile is based on the convolution between the Gaussian profile and the “full” Lorentzian profile which is just the classical Lorentz model without performing the traditional resonance approximation. It will be shown that the full Voigt profile can be computed based on two Faddeeva calculations, instead of just one as with the traditional Voigt profile. However, since most of the computations in a typical application can be performed under the full Lorentz approximation in very much the same way as have been described above, the approximation of the full Voigt profile is only slightly more complex in comparison to the approximation of the traditional Voigt profile.

The rest of the paper is organized as follows. In Section II is given a brief account on the “full” Lorentz profile, and its uniform convergence properties with respect to the traditional resonance approximation. In Section III is given the corresponding Voigt profiles, and in particular the “full” Voigt profile which can be expressed as a combination of two

Faddeeva calculations. The details of the derivation are given in the Appendix A. In Section IV is given the theorem which quantifies the uniform approximation properties of the Voigt profiles with regard to the corresponding Lorentz profiles. The details of the proof are given in the Appendix B. The subband adaptive line selection strategy is described in Section V and the numerical examples are given in Section VI. The paper is concluded with a short summary and a discussion.

II. THE CLASSICAL LORENTZ PROFILE

In a nonscattering atmosphere in the long wave regime, the absorption cross section k_ν of a molecule is the same as its extinction (or total) cross section σ_t . Based on the classical optical theorem [16, pp. 227–230, 272], [17, pp. 18–20] the absorption (extinction) cross section k_ν can then be modeled as

$$k_\nu = \text{Im}\{2\pi\nu\alpha\}, \quad (1)$$

where α is the polarizability, $\nu = \lambda^{-1}$ is the wavenumber and λ the wavelength in vacuum. This means that we can obtain the absorption coefficient as $k_\nu = \text{Im}\{h(\nu)\}$ where $h(\nu)$ is a Herglotz function¹ in the complex variable ν , and remember that it is really the extinction coefficient that we are modeling. Basic properties of Herglotz functions can be found in *e.g.*, [18], [19], [20], [21], [22]. Perhaps the most simple, and the most widely used model of the molecular polarizability is the classical Lorentz model

$$\alpha = S \frac{1}{\pi^2} \frac{1}{\nu_0^2 - \nu^2 - i2\gamma\nu}, \quad (2)$$

where S is the line strength, ν_0 the transition frequency (including the pressure shift) and γ the Half-Width-Half-Maximum (HWHM) parameter modeling the collision induced line broadening. Notably, the expression (2) can be derived by using a simple classical phenomenological model, as well as by using the more comprehensive perturbation techniques of quantum mechanics, see *e.g.*, [23, pp. 232–233], [24], [25, pp. 117], [26, pp. 104–108] and [27, pp. 1808–1809].

The Herglotz function modeling the line shapes in (1) is now given by

$$h(\nu) = \frac{2}{\pi} \frac{\nu}{\nu_0^2 - \nu^2 - i2\gamma\nu}, \quad (3)$$

and its imaginary part is

$$f_{\text{FL}}(\nu) = \text{Im}\{h(\nu)\} = \frac{4}{\pi} \frac{\gamma\nu^2}{(\nu_0^2 - \nu^2)^2 + 4\gamma^2\nu^2}. \quad (4)$$

Here, we will refer to (4) as the “full Lorentz” profile to distinguish it from the usual resonance approximation given below. The asymptotic behavior of (3) is readily found as

$$h(\nu) = \begin{cases} a_1\nu + o(\nu) & \text{as } \nu \rightarrow 0, \\ b_{-1}\nu^{-1} + o(\nu^{-1}) & \text{as } \nu \rightarrow \infty, \end{cases} \quad (5)$$

¹A Herglotz function $h(z)$ is a holomorphic function defined on the open upper half-plane $\mathbb{C}^+ = \{z \in \mathbb{C} | \text{Im}\{z\} > 0\}$ and where its imaginary part is non-negative, *i.e.*, $\text{Im}\{h(z)\} \geq 0$ for $z \in \mathbb{C}^+$.

where $o(\cdot)$ denotes the small ordo [28, p. 4] and where $a_1 = 2/\pi\nu_0^2$ and $b_{-1} = -2/\pi$. The Herglotz function in (3) is symmetric, and the following two sum rules [21] apply

$$\frac{2}{\pi} \int_0^\infty \text{Im}\{h(\nu)\} d\nu = -b_{-1} = \frac{2}{\pi}, \quad (6)$$

and

$$\frac{2}{\pi} \int_0^\infty \frac{\text{Im}\{h(\nu)\}}{\nu^2} d\nu = a_1 = \frac{2}{\pi\nu_0^2}. \quad (7)$$

The first sum rule in (6) establishes that the full Lorentz profile is normalized over $\mathbb{R}^+ = [0, \infty)$, and the second gives a sum rule relating the extinction cross section σ_t to the static polarizability of the line, $\int_0^\infty d\nu \sigma_t / \nu^2 = \pi^2 \alpha(0) = S/\nu_0^2$, cf., [24], [29], [30], [21].

The classical Lorentz profile used in most radiative transfer analysis is given by

$$f_L(\nu - \nu_0) = \frac{1}{\pi} \frac{\gamma}{(\nu - \nu_0)^2 + \gamma^2}, \quad (8)$$

see e.g., [31, p. 73], [12, p. 21-23], [32, pp. 263-266] and [10, Eq. (A14)]. The classical Lorentz profile above can readily be obtained as an approximation of (4) valid for ν close to resonance at ν_0 . It is emphasized, however, that (8) can also be derived from first principles, as in [5, pp. 77-78]. It is noticed that the convergence of the aforementioned approximation is somewhat subtle, in particular for small ν and small γ since $f_{FL}(0) = 0$ and $f_L(-\nu_0) = \gamma/\pi(\nu_0^2 + \gamma^2)$. To analyse this situation we consider the relative error

$$\begin{aligned} E_{\gamma, \nu_0}^{\text{FL}}(\nu) &= \frac{f_{FL}(\nu) - f_L(\nu - \nu_0)}{f_L(\nu - \nu_0)} \\ &= \frac{(\nu - \nu_0)^3(3\nu + \nu_0)}{(\nu_0 + \nu)^2(\nu_0 - \nu)^2 + 4\gamma^2\nu^2}, \end{aligned} \quad (9)$$

yielding the upper bound

$$|E_{\gamma, \nu_0}^{\text{FL}}(\nu)| \leq \frac{|\nu - \nu_0|(3\nu + \nu_0)}{(\nu_0 + \nu)^2}. \quad (10)$$

By assuming that $|\nu - \nu_0| \leq B$, it is readily seen that

$$|E_{\gamma, \nu_0}^{\text{FL}}(\nu)| \leq \frac{B\nu}{\nu_0^2} \leq \frac{B(\nu_0 + B)}{\nu_0^2} \quad \text{for } \nu > \nu_0 > 0, \quad (11)$$

and where $\nu < \nu_0 + B$, and

$$|E_{\gamma, \nu_0}^{\text{FL}}(\nu)| \leq \frac{B\nu_0}{\nu^2} \leq \frac{B(\nu + B)}{\nu^2} \quad \text{for } 0 < \nu < \nu_0, \quad (12)$$

and where $\nu_0 < \nu + B$. For a fixed bandwidth B_γ (related to the half-width γ) and $|\nu - \nu_0| \leq B_\gamma$, it is now readily seen that $E_{\gamma, \nu_0}^{\text{FL}}(\nu)$ converges uniformly to zero as $\nu_0 \rightarrow \infty$. It is emphasized that this result is merely a mathematical property of the line shapes which we will need later, and we do not intend to let the limit of large transition frequencies ν_0 violate the assumption about a non-scattering atmosphere.

For most practical purposes the analytically more tractable Lorentz profile (8) is an extremely good approximation of (4), except for some far wing calculations in the infrared windows where the density of spectral lines are very sparse. It may also be of interest to observe that the classical Lorentz profile

(8) is not symmetric, and hence does not correspond to a symmetric Herglotz function as would be physically expected in relation to the optical theorem (1), cf., [30], [21], [29]. In particular, since $f_L(-\nu_0) \neq 0$ there is no sum rule in the form of (7) relating the ν^{-2} moment of $f_L(\nu - \nu_0)$ to the static polarizability of the line.

III. VOIGT PROFILES

The classical Voigt profile is defined by the convolution integral

$$f_V(\nu) = \int_{-\infty}^\infty f_G(t) f_L(\nu - t) dt, \quad \nu \in \mathbb{R}, \quad (13)$$

where $f_G(\nu)$ is the Gaussian profile

$$f_G(\nu) = \sqrt{\frac{\ln 2}{\pi}} \frac{1}{\alpha} e^{-\nu^2 \ln 2 / \alpha^2}, \quad \nu \in \mathbb{R}, \quad (14)$$

modeling the Doppler broadening and where α is the corresponding HWHM parameter. Notice that the absorption line associated with the line center frequency ν_0 is given by the translation $f_V(\nu - \nu_0)$.

It is well known that the Voigt profile (13) can be computed by means of the Faddeeva function

$$w(z) = \frac{i}{\pi} \int_{-\infty}^\infty \frac{e^{-t^2}}{z - t} dt, \quad (15)$$

for which there exists many efficient numerical codes, see e.g., [13], [14], [15], [11]. In particular, by extending the integrand above with the complex conjugate of its denominator, it can be readily shown that

$$f_V(\nu) = \sqrt{\frac{\ln 2}{\pi}} \frac{1}{\alpha} \text{Im}\{iw(x + iy)\}, \quad (16)$$

where $x = \nu\sqrt{\ln 2}/\alpha$ and $y = \gamma\sqrt{\ln 2}/\alpha$. It may be noticed that $iw(z)$ is a symmetric Herglotz function generated by the Gaussian density, whereas $f_V(\nu - \nu_0)$ is the density of a non-symmetric (shifted) Herglotz function.

Now, we define also the “full Voigt” profile by

$$f_{FV}(\nu) = \int_{-\infty}^\infty f_G(t) f_{FL}(\nu - t) dt, \quad \nu \in \mathbb{R}, \quad (17)$$

where $f_{FL}(\nu)$ is the full Lorentz profile given by (4). In Appendix A is shown that the full Voigt profile can be computed by means of two Faddeeva calculations as $f_{FV}(\nu) = \text{Im}\{h_{FV}(\nu)\}$ where

$$\begin{aligned} h_{FV}(\nu) &= \sqrt{\frac{\ln 2}{\pi}} \frac{1}{\alpha} \left(\left(-\frac{\gamma}{a} + i \right) w \left((\nu + a + i\gamma) \frac{\sqrt{\ln 2}}{\alpha} \right) \right. \\ &\quad \left. + \left(\frac{\gamma}{a} + i \right) w \left((\nu - a + i\gamma) \frac{\sqrt{\ln 2}}{\alpha} \right) \right), \end{aligned} \quad (18)$$

and where $a = \sqrt{\nu_0^2 - \gamma^2}$ and $\nu_0 > \gamma$.

IV. UNIFORM APPROXIMATION OF VOIGT PROFILES

A. The classical Voigt profile

We define the relative error between the classical Voigt and Lorentz profiles as

$$E_{\alpha,\gamma}^V(\nu) = \frac{f_V(\nu) - f_L(\nu)}{f_L(\nu)}, \quad \nu \in \mathbb{R}, \quad (19)$$

and which can be manipulated to read

$$E_{\alpha,\gamma}^V(\nu) = \sqrt{\frac{\ln 2}{\pi}} \frac{1}{\alpha} \int_{-\infty}^{\infty} e^{-t^2 \ln 2 / \alpha^2} \frac{t(2\nu - t)}{\gamma^2 + (\nu - t)^2} dt, \quad (20)$$

which is an even function of ν . It is readily seen that $E_{\alpha,\gamma}^V(\nu) = \mathcal{O}\{\nu^{-1}\}$ for fixed values of α and γ and where $\mathcal{O}\{\cdot\}$ denotes the big ordo [28, p. 4]. Hence, for given values of α and γ the absolute error $|E_{\alpha,\gamma}^V(\nu)|$ will be arbitrarily small for sufficiently large ν . The superexponential Gaussian profile is furthermore highly localized and converges to the Dirac delta function as $\alpha \rightarrow 0$. Hence, we certainly have $\lim_{\alpha \rightarrow 0} f_V(\nu) = f_L(\nu)$ when γ and ν are fixed. However, as shown in the Appendix B, the convergence is in fact uniform over $\nu \in \mathbb{R}$ as $\alpha \rightarrow 0$ and γ is fixed. From the properties mentioned above it is now very close at hand to formulate the following theorem providing two simple statements, or criteria, for achieving a prescribed uniform error tolerance.

Theorem 4.1: For any $\epsilon > 0$ and $n_1 > 0$ there exists positive real numbers n_2 and n_3 such that the following two statements regarding the line parameters (α, γ) hold

$$\begin{cases} \gamma/\alpha > n_2 \Rightarrow \max_{\nu \in \mathbb{R}} |E_{\alpha,\gamma}^V(\nu)| < \epsilon \\ \gamma/\alpha > n_1 \Rightarrow \max_{|\nu| > n_3\alpha} |E_{\alpha,\gamma}^V(\nu)| < \epsilon. \end{cases} \quad (21)$$

The lower limit relating to $\gamma/\alpha > n_1$ above is probably not needed as n_1 can be chosen to be arbitrarily small, but is included here with the purpose of simplifying the proof of the theorem. In addition, in a practical application the parameter γ/α is always bounded from below by a nonzero number n_1 . The Theorem 4.1 will be proved below, but let us first give a few comments on its application.

For a given set of line parameters (α, γ) the first statement in (21) is the stronger one, and it can be used as a criterion to determine whether the Voigt profile can be approximated by the Lorentz profile within the given error tolerance ϵ on the whole of the frequency axis $\nu \in \mathbb{R}$. If the condition in the first statement is not satisfied, then the second (weaker) statement asserts that it is sufficient to calculate the Voigt profile within the (usually very small) limited frequency range $|\nu| \leq n_3\alpha$, and hence that the Lorentz profile can be used for $|\nu| > n_3\alpha$. The practical usefulness of the theorem stems from the fact that it is numerically much more efficient to calculate the Lorentz profile in comparison to the Voigt profile, and that simple comparative conditions such as $|\nu| \leq n_3\alpha$ above can readily be implemented in software by using sorting routines at very low computational cost. The application of Theorem 4.1 can now be summarized as follows. Assume that $\epsilon > 0$ and $\gamma/\alpha > n_1$. Then there are positive real numbers n_2 and

n_3 such that the following criteria can be applied to the line parameters (α, γ)

$$\begin{cases} \gamma/\alpha > n_2 \Rightarrow \text{Use the Lorentz profile for all } \nu \\ \gamma/\alpha < n_2 \Rightarrow \text{Use the Lorentz profile for } |\nu| > n_3\alpha \\ \text{and the Voigt profile for } |\nu| < n_3\alpha, \end{cases} \quad (22)$$

which guarantees that the approximation error $|E_{\alpha,\gamma}^V(\nu)| < \epsilon$ for all $\nu \in \mathbb{R}$.

To prove Theorem 4.1 it is convenient to normalize (20) using the substitution $t\sqrt{\ln 2}/\alpha \leftrightarrow t$ to yield

$$E_{\alpha,\gamma}^V(\nu) = \frac{1}{\sqrt{\pi}} \int_{-\infty}^{\infty} e^{-t^2} \frac{t(2\tilde{\nu} - t)}{\tilde{\gamma}^2 + (\tilde{\nu} - t)^2} dt = E_{\tilde{\alpha},\tilde{\gamma}}^V(\tilde{\nu}), \quad (23)$$

and where we have introduced the dimensionless parameters

$$\tilde{\alpha} = \sqrt{\ln 2}, \quad \tilde{\gamma} = \frac{\gamma}{\alpha} \sqrt{\ln 2}, \quad \tilde{\nu} = \frac{\nu}{\alpha} \sqrt{\ln 2}. \quad (24)$$

In Appendix B below is shown that the expression (23) converges to zero uniformly over $\tilde{\nu} \in \mathbb{R}$ as $\tilde{\gamma} \rightarrow \infty$, and hence that

$$\lim_{\gamma/\alpha \rightarrow \infty} \max_{\nu \in \mathbb{R}} |E_{\alpha,\gamma}^V(\nu)| = \lim_{\tilde{\gamma} \rightarrow \infty} \max_{\tilde{\nu} \in \mathbb{R}} |E_{\tilde{\alpha},\tilde{\gamma}}^V(\tilde{\nu})| = 0. \quad (25)$$

The result (25) asserts the validity of the first statement in Theorem 4.1. From the error bound (62) derived in Appendix B it is furthermore seen that $|E_{\tilde{\alpha},\tilde{\gamma}}^V(\tilde{\nu})|$ is uniformly bounded by an arbitrary $\epsilon > 0$ for $\tilde{\gamma} > n_1\sqrt{\ln 2}$ where $n_1 > 0$ is fixed and the normalized frequency $|\tilde{\nu}|$ is sufficiently large. This is also consistent with the observation that $E_{\tilde{\alpha},\tilde{\gamma}}^V(\tilde{\nu}) = \mathcal{O}\{\tilde{\nu}^{-1}\}$ for large $\tilde{\nu}$, and which can be seen directly from (23). Hence, there exists a positive number n_3 such that

$$|E_{\tilde{\alpha},\tilde{\gamma}}^V(\tilde{\nu})| < \epsilon \quad \text{for } |\tilde{\nu}| > n_3\sqrt{\ln 2}, \quad (26)$$

or equivalently

$$|E_{\alpha,\gamma}^V(\nu)| < \epsilon \quad \text{for } |\nu| > n_3\alpha, \quad (27)$$

and where $\gamma/\alpha > n_1$. The result (27) finally asserts the validity of the second statement in Theorem 4.1.

The uniform error bounds (61) and (62) derived in Appendix B are useful to prove the validity of the two statements in (21), but the bounds are not particularly sharp. However, since the normalized form of the relative error defined in (23) can be represented by the single parameter $\tilde{\gamma}$, we can readily find approximate values of n_2 and n_3 yielding sharp error bounds by direct numerical calculation of (19) for various values of γ/α .

In Fig. 1 is shown a computation of the relative error $|E_{\alpha,\gamma}^V(\nu)|$ defined via (19) and (24), plotted here as a function of the normalized frequency ν/α for $\gamma/\alpha = 10^{-3}, 1, 10, 30$. The Voigt profile is computed based on (16) and where the Faddeeva function (15) has been implemented in Matlab using the software described in [13], [14]. As can be seen in this plot, there is a local maximum around ± 1 for small values of $\gamma/\alpha < 1$, and around $\pm \gamma/\alpha$ (in fact around $\pm 1.075\gamma/\alpha$) for large values of $\gamma/\alpha > 1$. This means that we now have full numerical control over the localization of extremal

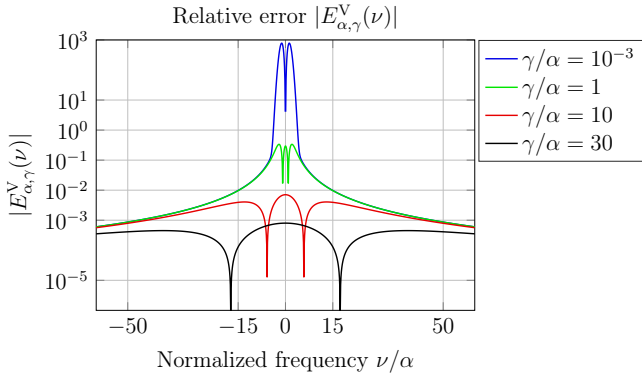


Fig. 1. Computation of the relative error $|E_{\alpha,\gamma}^V(\nu)|$ between the Voigt profile and the Lorentz profile. The error is plotted here as a function of the normalized frequency ν/α for $\gamma/\alpha = 10^{-3}, 1, 10, 30$.

values when executing the numerical study. Each plot in Fig. 1 is made with 2000 frequency points in the interval $\nu/\alpha \in [-60, 60]$, which is a sufficient resolution for our purposes here.

In a typical application of broadband radiative transfer in the atmosphere (see the numerical examples below), the normalized pressure broadening is $\gamma/\alpha > 10^{-3}$. With reference to the Theorem 4.1, we can now infer from Fig. 1 that the parameter choices $n_1 = 10^{-3}$ together with $(n_2, n_3) = (10, 15)$ and $(n_2, n_3) = (30, 50)$ will guarantee a relative error less than $\epsilon = 10^{-2}$ and $\epsilon = 10^{-3}$, respectively.

B. The full Voigt profile

Similar as above we can now define the relative error between the full Voigt and the full Lorentz profiles as

$$E_{\alpha,\gamma,\nu_0}^{\text{FV}}(\nu) = \frac{f_{\text{FV}}(\nu) - f_{\text{FL}}(\nu)}{f_{\text{FL}}(\nu)}, \quad \nu \in \mathbb{R}, \quad (28)$$

and which can be manipulated to read

$$E_{\alpha,\gamma,\nu_0}^{\text{FV}}(\nu) = \sqrt{\frac{\ln 2}{\pi}} \frac{1}{\alpha} \int_{-\infty}^{\infty} e^{-t^2 \ln 2 / \alpha^2} \frac{t(2\nu - t)(\nu^4 - \nu_0^4 - \nu^2 t(2\nu - t))}{((\nu_0^2 - (\nu - t)^2)^2 + 4\gamma^2(\nu - t)^2) \nu^2} dt, \quad (29)$$

which is an even function of ν . The expression (29) is obviously more involved than (20), but it could of course be analyzed in a similar manner as with the classical Voigt profile described in the Appendix B. However, this is not necessary at this point, as we can now employ more simple arguments to establish its convergence as follows. First, it is noticed that the expression (29) is singular at $\nu = 0$, which of course is natural since $f_{\text{FL}}(0) = 0$ but $f_{\text{FV}}(0) \neq 0$. Hence, we can not have uniform convergence on the whole of \mathbb{R} . Secondly, we have now one more parameter to consider, the line center

frequency ν_0 . We therefore proceed as above, and rewrite (29) by using the substitution $t\sqrt{\ln 2}/\alpha \leftrightarrow t$, yielding

$$E_{\alpha,\gamma,\nu_0}^{\text{FV}}(\nu) = \frac{1}{\sqrt{\pi}} \int_{-\infty}^{\infty} e^{-t^2} \frac{t(2\tilde{\nu} - t)(\tilde{\nu}^4 - \tilde{\nu}_0^4 - \tilde{\nu}^2 t(2\tilde{\nu} - t))}{((\tilde{\nu}_0^2 - (\tilde{\nu} - t)^2)^2 + 4\tilde{\gamma}^2(\tilde{\nu} - t)^2) \tilde{\nu}^2} dt = E_{\tilde{\alpha},\tilde{\gamma},\tilde{\nu}_0}^{\text{FV}}(\tilde{\nu}), \quad (30)$$

where we have introduced the dimensionless parameters

$$\tilde{\alpha} = \sqrt{\ln 2}, \quad \tilde{\gamma} = \frac{\gamma}{\alpha} \sqrt{\ln 2}, \quad \tilde{\nu} = \frac{\nu}{\alpha} \sqrt{\ln 2}, \quad \tilde{\nu}_0 = \frac{\nu_0}{\alpha} \sqrt{\ln 2}. \quad (31)$$

The scaling introduced above means that it is sufficient to consider the uniform approximation properties of (30) over the normalized frequencies $|\tilde{\nu} - \tilde{\nu}_0| < \tilde{B}$, and study how the approximation error behaves for a range of values of $\tilde{\gamma}$ as $\tilde{\nu}_0 \rightarrow \infty$. As a mathematical argument for this procedure, we can now employ the convergence of the full Lorentz profile $f_{\text{FL}}(\nu) \rightarrow f_{\text{L}}(\nu - \nu_0)$ which is uniform for $|\nu - \nu_0| < B$ as $\nu_0 \rightarrow \infty$, cf., the derivation of (11) and (12) in Section II. Due to the convolution with the Gaussian profile, we immediately have also that $f_{\text{FV}}(\nu) \rightarrow f_{\text{V}}(\nu - \nu_0)$ as well as $E_{\alpha,\gamma,\nu_0}^{\text{FV}}(\nu) \rightarrow E_{\alpha,\gamma}^{\text{V}}(\nu - \nu_0)$, and which are uniform for $|\nu - \nu_0| < B$ as $\nu_0 \rightarrow \infty$.

The uniform approximation procedure is illustrated in Figs. 2 and 3. As can be seen in these plots, the full Voigt error $E_{\alpha,\gamma,\nu_0}^{\text{FV}}(\nu)$ is locally very similar to the Voigt error $E_{\alpha,\gamma}^{\text{V}}(\nu - \nu_0)$ of Fig. 1 already at $\nu_0/\alpha = 100$, and almost identical at $\nu_0/\alpha = 300$ (excluding the region close to the origin). In a typical application of broadband radiative transfer in the atmosphere (see the numerical examples below), the normalized center frequency is in the order of $\nu_0/\alpha > 10^5$. Hence, assuming (or checking) that ν_0/α is sufficiently large with reference to the analysis illustrated in Figs. 2 and 3 above, it is safe to employ the same Theorem 4.1, the same approximation procedure (22) and the same criteria parameters n_1 and (n_2, n_3) in connection with the full Voigt profile, as with the classical Voigt profile. The only difference is that the approximation is now valid over some finite region with bandwidth B , including the transition frequency ν_0 and excluding a suitable neighborhood of the origin.

V. ADAPTIVE LINE SELECTION

Even when using the fast approximation of Voigt profiles as expressed in (22) above, the broadband line-by-line calculations of interest in radiative transfer analysis may still be computationally huge and therefore impractical. Hence, it is of interest to make the computations faster and more effective by reducing the number of spectral lines that are included in the computations and only employ the lines that are necessary and relevant at each frequency. There is no simple rule to make this line selection as efficient as possible in order to achieve some required accuracy. However, based on the approximation theory that has been developed above we will outline here a simple, pragmatic and readily programmable criterion to make an adaptive line selection using only a few adjustable parameters to control the accuracy. The method is obviously

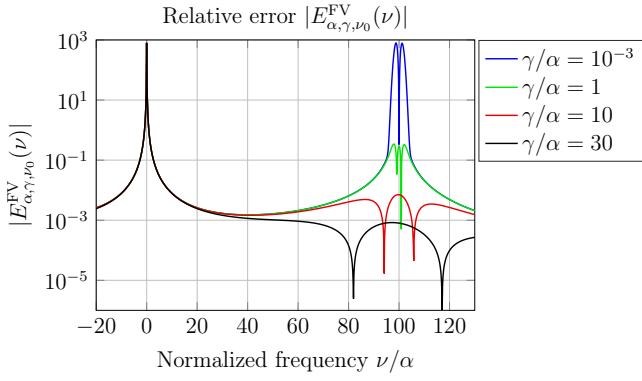


Fig. 2. Computation of the relative error $|E_{\alpha, \gamma, \nu_0}^{FV}(\nu)|$ between the full Voigt profile and the full Lorentz profile. The error is plotted here as a function of the normalized frequency ν/α for $\gamma/\alpha = 10^{-3}, 1, 10, 30$. The center frequency is $\nu_0/\alpha = 100$.

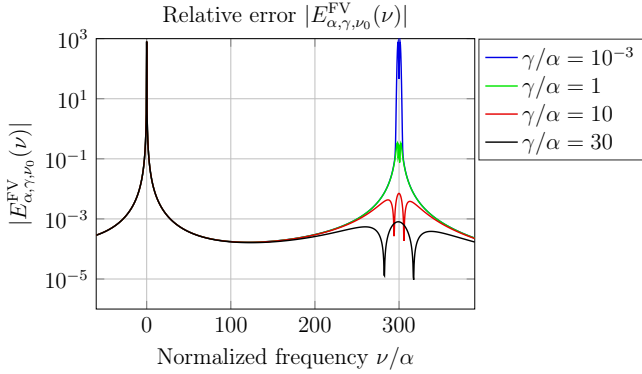


Fig. 3. Same plot as in Fig. 2, except here the center frequency has been increased to $\nu_0/\alpha = 300$.

suboptimal, but it is able to significantly reduce the number of spectral line calculations that are included based on simple and comprehensible criteria while at the same time maintaining a high computational accuracy.

We consider the calculation of the absorption coefficient k_ν expressed as

$$k_\nu = \sum_j S_j f_j(\nu), \quad (32)$$

where S_j are the line strengths and $f_j(\nu)$ the approximate Voigt profiles as described in (22). An individual spectral profile in (32) is denoted $k_{\nu_j}(\nu) = S_j f_j(\nu)$, and which is associated with a specific transition frequency ν_j (including pressure shift), and line parameters γ_j and α_j , all of which depend on height (temperature and pressure) in the atmosphere. It is assumed that $\gamma_j/\alpha_j > n_1$ for all j and where n_1 is the parameter defined in Theorem 4.1. We will adopt here a block processing approach where the whole computational domain is divided into subdomains of relatively small and manageable sizes. Hence, we will consider the calculation of the absorption coefficient k_ν over a fixed and relatively narrow subinterval $\Omega = [\nu_a, \nu_b]$, and estimate the contribution from all the individual spectral lines where $k_{\nu_j}(\nu) = S_j f_j(\nu)$ for $j = 1, \dots, J$.

We start by defining the minimum distance between the transition frequency ν_j and the set Ω as

$$D_j = \begin{cases} \min\{|\nu_a - \nu_j|, |\nu_b - \nu_j|\} & \text{if } \nu_j \notin \Omega, \\ 0 & \text{if } \nu_j \in \Omega, \end{cases} \quad (33)$$

for all $j = 1, \dots, J$. Now, it is readily seen that for $D_j > n_3 \alpha_j$ the following implication holds

$$\begin{aligned} \nu \in \Omega &\Rightarrow n_3 \alpha_j < D_j \leq |\nu - \nu_j| \\ &\Rightarrow S_j \frac{1}{\pi} \frac{\gamma_j}{\gamma_j^2 + D_j^2} > S_j \frac{1}{\pi} \frac{\gamma_j}{\gamma_j^2 + |\nu - \nu_j|^2} \approx k_{\nu_j}(\nu), \end{aligned} \quad (34)$$

where ν_j is outside of Ω and where the last approximation is due to the Theorem 4.1 and the criterion in (22).

For subintervals Ω which contain at least one spectral line j , we define the largest self-contribution over Ω as

$$k_{\max}^{\text{int}} = \max_{\nu_j \in \Omega} k_{\nu_j}(\nu_j) = \max_{\nu_j \in \Omega} S_j f_j(\nu_j), \quad (35)$$

which is a reasonable computational task based on the ordinary Voigt profile implemented by using *e.g.*, [13]. Based on (34) we can also estimate the largest contribution to k_ν from spectral lines j outside of Ω as

$$k_{\max}^{\text{ext}} = \max_{D_j > n_3 \alpha_j} S_j \frac{1}{\pi} \frac{\gamma_j}{\gamma_j^2 + D_j^2}, \quad (36)$$

and where the condition $D_j > n_3 \alpha_j$ guarantees that the Lorentz approximation is valid for $\nu \in \Omega$. An estimate of the largest contribution from any individual spectral line to k_ν is now given by $k_{\max} = \max\{k_{\max}^{\text{int}}, k_{\max}^{\text{ext}}\}$. If Ω does not contain any spectral lines j , we simply choose $k_{\max} = k_{\max}^{\text{ext}}$. It is now readily seen that $k_{\nu_j}(\nu) \leq k_{\max}$ for $\nu \in \Omega$ and for all j such that $\nu_j \in \Omega$ or $D_j > n_3 \alpha_j$.

We now decide to exclude all the spectral lines with

$$D_j > n_3 \alpha_j \quad \text{and} \quad S_j \frac{1}{\pi} \frac{\gamma_j}{\gamma_j^2 + D_j^2} < k_{\max} A, \quad (37)$$

where A is a small positive number. From (34), we see that for those lines it will hold that $k_{\nu_j}(\nu) < k_{\max} A$ for all $\nu \in \Omega$. It is finally observed that the criterion in (37) is also equivalent to include all the spectral lines satisfying

$$D_j < n_3 \alpha_j \quad \text{or} \quad S_j \frac{1}{\pi} \frac{\gamma_j}{\gamma_j^2 + D_j^2} > k_{\max} A. \quad (38)$$

It is noted that lines satisfying $D_j < n_3 \alpha_j$ are always included, *i.e.*, all lines inside or in a close neighborhood of Ω . It is also very useful to put an upper bound $K \ll J$ on the number of lines satisfying both $D_j > n_3 \alpha_j$ as well as the second criterion in (38) organized in descending order. The calculations in (33), (35) and (36) as well as the criterion (38) can now be readily implemented in a computer code.

The extension of the procedure outlined above to the case with the full Voigt profile is straightforward. This means *e.g.*, that the sequence

$$\hat{f}_j = \frac{1}{\pi} \frac{\gamma_j}{\gamma_j^2 + D_j^2} \quad (39)$$

should be replaced for the sequence

$$\hat{f}_j = \begin{cases} \frac{4}{\pi} \frac{\gamma_j \nu_b^2}{(\nu_a^2 - \nu_j^2)^2 + 4\gamma_j^2 \nu_a^2} & \text{for } \nu_j < \nu_a \\ \frac{4}{\pi} \frac{\gamma_j \nu_b^2}{(\nu_j^2 - \nu_b^2)^2 + 4\gamma_j^2 \nu_a^2} & \text{for } \nu_j > \nu_b, \end{cases} \quad (40)$$

which will guarantee that $S_j \hat{f}_j > k_{\nu_j}(\nu)$ for $\nu \in \Omega$ and $D_j > n_3 \alpha_j$, similar as in (34). In practice, this modification of \hat{f}_j is scarcely needed in view of the very small approximation error between the Voigt and the full Voigt profiles. The important modification here is to replace the calculation of the classical Lorentz profile with the calculation of the full Lorentz profile in the implementation of (22).

VI. NUMERICAL EXAMPLES

As a simple benchmark problem for comparing the accuracy and computational effort associated with the proposed profile approximations, we consider here a broadband line-by-line analysis of radiative transfer in the atmosphere. The computer code is implemented in Matlab and executed on a standard laptop. It is emphasized that the code has not been optimized for speed. It is merely a straightforward implementation of a simple recursive algorithm with the aim of comparing the different approximation methods on equal terms.

We consider the computation of the outgoing monochromatic irradiance F_ν transmitted by the Earth at 65 km height in a representative, plane-parallel and piece-wise homogeneous atmosphere, as depicted in Fig. 4. The pressure profile is implemented as the exponential law of an isothermal atmosphere [33, Eq. (4.24)] based on the mean value of the temperature profile shown in the figure. A recursive solution of the corresponding transfer equation for thermal IR radiation in a non-scattering atmosphere [12, Eq. (4.2.2)] is given by

$$I_\nu(z_{i+1}, \mu) = I_\nu(z_i, \mu) e^{-d_i \sum_s N^{(s)}(z_i) k_\nu^{(s)}(z_i) / \mu} + B_\nu(T(z_i)) \left(1 - e^{-d_i \sum_s N^{(s)}(z_i) k_\nu^{(s)}(z_i) / \mu} \right), \quad (41)$$

for $i = 1, \dots, 65$. Here, $I_\nu(z_i, \mu)$ are the radiances at height z_i and direction $\mu = \cos \theta$, $z_i = (i - 1) \cdot 1$ km, $d_i = z_{i+1} - z_i$, $N^{(s)}(z_i)$ the number density of each species (s), $k_\nu^{(s)}(z_i)$ the corresponding absorption coefficients and $B_\nu(T(z_i))$ the Plack function of blackbody radiation at temperature $T(z_i)$. The iteration is started at $z = 0$ with temperature $T = 288$ K.

Five different species (s) are included in the computation comprising a total of 430070 transitions in the range 0-3000 cm^{-1} , cf., Table I. The line parameters are taken from the HITRAN data base [9], [10], [34] and the following six different profile computations are considered: The Voigt (V) profile (13) and the full Voigt (FV) profile (17) are based on the Faddeeva function as in (16) and (18), respectively, and implemented by using [13]. The corresponding approximations, the fast Voigt (fV) profile and the fast full Voigt (ffV) profile are based on (22), and their combinations with the adaptive line selection procedures (fV+LS and ffV+LS) are described in Section V. The parameter setting for both

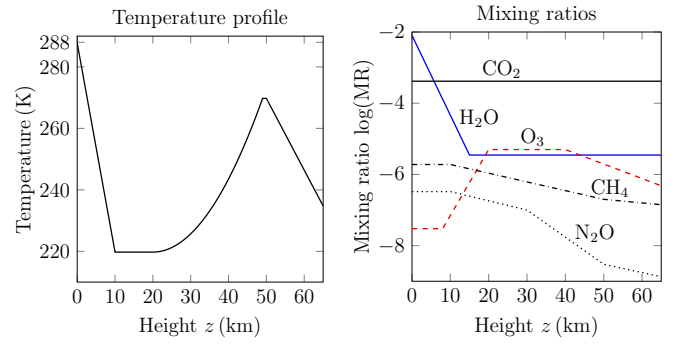


Fig. 4. Representative vertical profiles of temperature and mixing ratios for the five most important greenhouse gases in midlatitude regions according to [12, Figs. 3.1 and 3.2].

Constituent	Isotopologue	# lines 0-3000 cm^{-1}
Water vapor	H_2^{16}O	19615
Carbon dioxide	$^{12}\text{C}^{16}\text{O}_2$	68829
Ozone	$^{16}\text{O}_3$	210144
Methane	$^{12}\text{CH}_4$	110415
Nitrous oxide	$^{14}\text{N}_2^{16}\text{O}$	21067
Total # lines		430070

TABLE I
THE ISOTOPOLOGUES OF THE SPECIES THAT HAVE BEEN INCLUDED IN THE MODELING AND THE CORRESPONDING NUMBER OF TRANSITIONS THAT ARE AVAILABLE IN THE HITRAN DATABASE OVER THE BANDWIDTH 0-3000 cm^{-1} .

of the fast Voigt procedures implemented as in (22) are here $n_1 = 10^{-3}$ and $(n_2, n_3) = (10, 15)$ for a maximum of 1% relative approximation error. The adaptive line selection is implemented with parameters $A = 10^{-8}$ and $K = 1000$, see Section V.

The full bandwidth of the computation is 100-2000 cm^{-1} and which is divided into blocks of 2000 frequency points each. The frequency resolution of each block is set by the Doppler broadening of the heaviest species (ozone) at the lowest temperature (220 K) yielding a total of 1955 blocks and $3.91 \cdot 10^6$ frequency points over the whole bandwidth. For each frequency block Ω , the iteration in (41) is implemented as an array of 2000×10 values of radiances evaluated at 2000 Gauss-Legendre nodes $\nu \in \Omega$ and 10 Gauss-Legendre nodes $\mu \in (0, 1)$. The integration of the total irradiance of each block is then conveniently executed by using the corresponding Gauss-Legendre weights. The resulting monochromatic irradiance at $z = 65$ km is then finally evaluated as the total irradiance per frequency block, as depicted in Fig. 5. The frequency resolution of the monochromatic irradiance shown in the figure is hence varying from 0.15 cm^{-1} to 3.1 cm^{-1} . Note however that the resolution of the computation in (41) is 2000 times more dense, i.e., the resolution varies here between 0.000075 cm^{-1} and 0.0015 cm^{-1} . The result shown in Fig. 5 is based on the fast Voigt profile with adaptive line selection (fV+LS) as expressed in (16), (22) and (38). The computation time on a standard laptop is about 3-4 hours.

In Figs. 6 and 7 are shown the corresponding irradiance calculations for some of the profiles as mentioned above,

and which are evaluated here in the two narrow bands 667-668 cm^{-1} and 900-901.4 cm^{-1} , comprising 2000 frequency points each. The Voigt (V) and full Voigt (FV) profiles are not shown here since they are indistinguishable from the fast approximations (fV) and (fFV) and which are hence very accurate in these examples. In Fig. 6 we can see that there are many closely spaced absorption lines in the 667 cm^{-1} band, and there is therefore virtually no difference between the Voigt and the full Voigt profiles, and the latter are therefore not shown in this plot. As we can see, there is only a small deviation between the fast Voigt (fV) and the fast Voigt with adaptive line selection (fV+LS) in this band.

In Fig. 7 we can see that there are very few absorption lines in the 900 cm^{-1} band, and the far wings are therefore of more importance. There is therefore a small difference between the Voigt and the full Voigt profiles, and there is also a small deviation using the line selection procedure. The computer time and relative errors (relative V and FV, respectively) of these calculations are summarized in Table II. The accuracy in these calculations can readily be improved by tuning the convergence parameters (n_2, n_3), A and K described above, and which hence can be traded against the corresponding increase in computer time.

The total number of line calculations that are available in the numerical algorithm described above is $430070 (\text{lines}) \cdot 65 (\text{heights}) \cdot 1955 (\text{blocks}) \approx 5.5 \cdot 10^{10}$, each absorption line evaluation comprising 2000 frequency points. Furthermore, each of the 1955 block calculations at each of the 65 heights also consists of an evaluation of the radiance at the 2000 frequency points in 10 different directions, and then followed by the associated Gauss-Legendre integration. Based on the timings presented in Table II, it can be estimated that a computation of the spectra as shown in Fig. 5 based on the Voigt profile without approximations will take about 220 days, and about twice this time using the full Voigt profile since it requires two Faddeeva evaluations instead of just one. By using the fast Voigt (fV) approximation (22) the computer time for calculating all lines reduces to about 7 days. Finally, by using the adaptive line selection criteria (fV+LS) (38) the number of line calculations reduces from a total of $5.5 \cdot 10^{10}$ to about $4.8 \cdot 10^8$ corresponding to about 0.88 % of all the available line calculations. The final computation time on a standard laptop is now 3-4 hours.

VII. SUMMARY AND CONCLUSIONS

This paper presents uniform error bounds for fast calculation of approximate Voigt profiles. The purpose is to accelerate the computationally huge broadband line-by-line analysis of radiative transfer in the atmosphere. The main idea is to replace the relatively demanding Voigt calculations for the much simpler and faster Lorentz calculations whenever this can be done within a given error tolerance. In addition, it is also demonstrated how the uniform bounds enable a fast and efficient subband adaptive line selection strategy that includes only the spectral lines that give the most significant contribution to the absorption coefficient. Numerical examples

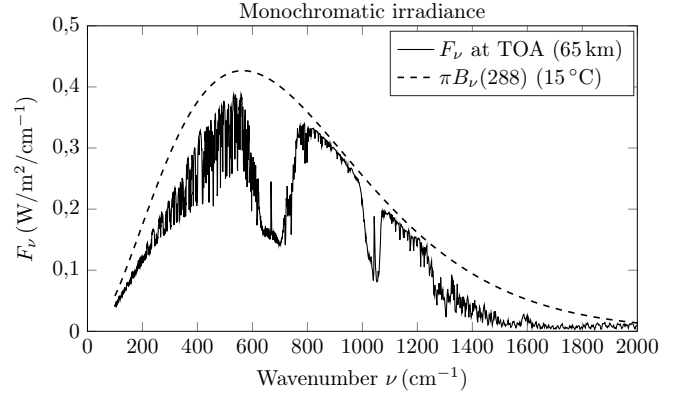


Fig. 5. A computation of the outgoing monochromatic irradiance F_ν transmitted by the Earth at 65 km height. The computation is based on the fast Voigt approximation and the adaptive line selection procedure (fV+LS). The dashed line shows the corresponding blackbody radiation $\pi B_\nu(T)$ at temperature $T = 288$ K.

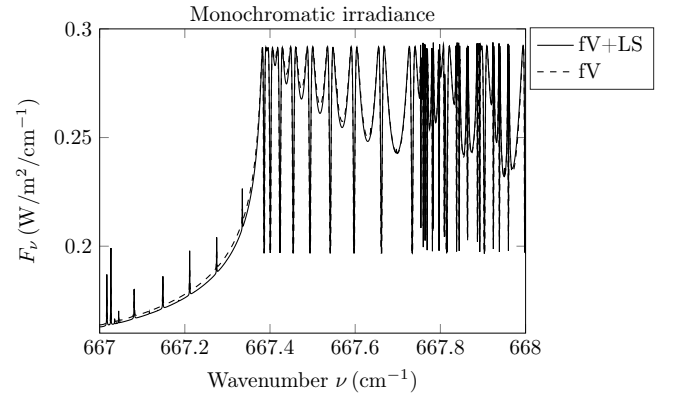


Fig. 6. The outgoing monochromatic irradiance F_ν as in Fig. 5, evaluated here in the band 667-668 cm^{-1} . The computations are based on the fast Voigt (fV) approximation as well as the combination with the adaptive line selection procedure (fV+LS), respectively.

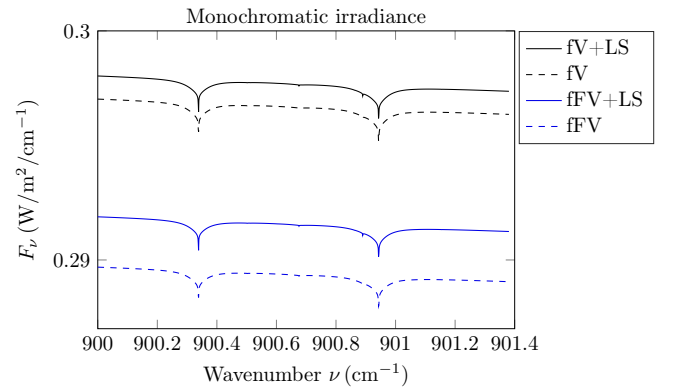


Fig. 7. The outgoing monochromatic irradiance F_ν as in Fig. 5, evaluated here in the band 900-901.4 cm^{-1} . The computations are based on the fast Voigt (fV) as well as the fast full Voigt (fFV) approximations, and as combinations with the adaptive line selection procedure (fV+LS, or fFV+LS), respectively.

Band (cm ⁻¹)	Profile	Time (s)	rel. error
667-668	fV+LS	6	5.7 · 10 ⁻³
667-668	fV	329	8.3 · 10 ⁻⁵
667-668	V	9268	—
667-668	fFV+LS	8	5.7 · 10 ⁻³
667-668	fFV	327	8.3 · 10 ⁻⁵
667-668	FV	23196	—
900-901.4	fV+LS	7	3.4 · 10 ⁻³
900-901.4	fV	315	7.4 · 10 ⁻⁹
900-901.4	V	9664	—
900-901.4	fFV+LS	8	7.6 · 10 ⁻³
900-901.4	fFV	324	7.2 · 10 ⁻⁹
900-901.4	FV	23953	—

TABLE II

REQUIRED COMPUTER TIME ON A STANDARD LAPTOP AND RELATIVE APPROXIMATION ERRORS IN THE COMPUTATION OF THE TOTAL IRRADIANCE BASED ON THE 2000 FREQUENCY POINTS SHOWN IN FIGS. 6 AND 7 AND THE 430070 LINES LISTED IN TABLE I. THE REFERENCE COMPUTATION CORRESPONDING TO THE VOIGT (V) AND FULL VOIGT (FV) PROFILES ARE BASED ON [13].

are included to illustrate that the two approaches can accelerate the line-by-line computations by several orders of magnitude with very little loss in accuracy.

A new “full” Voigt profile is also presented based on the “full” Lorentz profile, and which is obtained without making the traditional resonance approximation. The full Lorentz profile can be very well motivated from the classical principles of molecular polarizabilities, optical theorems and associated sum rules connecting to the static polarizability. On the other hand, the classical Lorentz resonance approximation can also be derived directly from first principles based on quantum mechanics, as in [5, pp. 77-78]. Hence, more research is needed to explore the potential application of this new (old!) profile. In particular, the full Voigt profile is potentially suitable for far wing (off resonance) calculations in spectral regions where line mixing effects can be ignored. Based on the numerical examples of broadband radiative transfer in the atmosphere that are presented here, we can see that there is a slight discrepancy in the computed irradiances at high altitude when using the Voigt and the full Voigt profiles, respectively. These discrepancies are furthermore most significant in the so called “infrared windows”, where the density of spectral lines is sparse and the far wing contributions are of more importance.

As a future potential of employing the approximation techniques that have been presented in this paper, it may be of interest to explore their use to increase the accuracy and efficiency of existing line-by-line algorithms, see *e.g.*, [8]. It may also be of interest to explore their extension to be used with existing line mixing methods [1], [2], [3], [4], [7], as well as with the new line shapes based on partial correlation, speed dependency and velocity changes that have been developed recently, see *e.g.*, [6], [11]. It can be expected that, while advanced methods are employed for narrow inband calculations, it may be possible to approximate the far wing contributions by using adequate asymptotics based on simple

functions, error estimates as well as pre-calculated and stored data. The aim of these studies would be to render the new, more accurate line shapes and line mixing formulas more applicable for computationally huge broad-band line-by-line analysis of radiative transfer in the atmosphere.

APPENDIX

A. The full Voigt profile

To show the result (18) we will employ the analytic Fourier (Laplace) transform

$$F(\omega) = \mathcal{F}\{f(t)\} = \int_{-\infty}^{\infty} f(t)e^{-i\omega t} dt \quad (42)$$

with inverse

$$f(t) = \mathcal{F}^{-1}\{F(\omega)\} = \frac{1}{2\pi} \int_{-\infty+i y}^{\infty+i y} F(\omega)e^{i\omega t} d\omega, \quad (43)$$

where $\omega = x + iy$ and the contour integral is carried out inside the region of analyticity of $F(\omega)$. We will make use of the following standard transforms

$$\mathcal{F}\{\sin(at)u(t)\} = \frac{a}{a^2 - \omega^2} \quad (44)$$

$$\mathcal{F}\{-i \cos(at)u(t)\} = \frac{\omega}{a^2 - \omega^2} \quad (45)$$

$$\mathcal{F}\left\{\sqrt{\frac{b}{\pi}} e^{i\omega_0 t} e^{-bt^2}\right\} = e^{-(\omega - \omega_0)^2 / 4b} \quad (46)$$

where a and b are positive real constants, ω_0 a complex valued constant and $u(t)$ the unit step (Heaviside) function. The region of analyticity of (44) and (45) is $\text{Im}\{\omega\} < 0$ and for (46) it is the whole of \mathbb{C} . We will furthermore employ the following analytic form of the Parseval’s relation

$$\int_{-\infty}^{\infty} f(t)g^*(t) dt = \frac{1}{2\pi} \int_{-\infty+i y}^{\infty+i y} F(\omega)G^*(\omega^*) d\omega, \quad (47)$$

which can be derived directly by using (43) and where $(\cdot)^*$ denotes the complex conjugate and $y > 0$ is fixed. The contour integral in (47) extends along the real line ($d\omega = dx$) in the upper half of the complex plane and requires (at least) that $F(\omega)$ is analytic in a neighborhood of the line $\omega = +iy$ in the upper half plane and that $G(\omega)$ is analytic in a neighborhood of the line $\omega = -iy$ in the lower half.

In order to derive (18), we start from (17) and write

$$\begin{aligned} f_{\text{FV}}(\nu) &= f_{\text{G}}(\nu) * f_{\text{FL}}(\nu) \\ &= \sqrt{\frac{\ln 2}{\pi}} \frac{1}{\alpha} e^{-\nu^2 \ln 2 / \alpha^2} * \text{Im} \left\{ \frac{2}{\pi} \frac{\nu}{\nu_0^2 - \nu^2 - i2\gamma\nu} \right\} \end{aligned} \quad (48)$$

where $*$ denotes convolution and where (3), (4) and (14) have been used. This means that we can write $f_{\text{FV}}(\nu) = \text{Im} \{h_{\text{FV}}(\nu)\}$ where

$$h_{\text{FV}}(\nu) = \sqrt{\frac{\ln 2}{\pi}} \frac{2}{\pi\alpha} \int_{-\infty}^{\infty} e^{-(\nu-x)^2 \ln 2 / \alpha^2} \frac{x dx}{\nu_0^2 - x^2 - i2\gamma x}. \quad (49)$$

By introducing $\omega = x + i\gamma$, $\omega_0 = \nu + i\gamma$, $a^2 = \nu_0^2 - \gamma^2$ and $b = \alpha^2/4 \ln 2$, the integral above can be written

$$\begin{aligned} I &= \int_{-\infty}^{\infty} e^{-(\nu-x)^2 \ln 2 / \alpha^2} \frac{x dx}{\nu_0^2 - x^2 - i2\gamma x} \\ &= \int_{-\infty+i\gamma}^{\infty+i\gamma} e^{-(\omega-\omega_0)^2 \ln 2 / \alpha^2} \frac{\omega - i\gamma}{a^2 - \omega^2} d\omega \\ &= \int_{-\infty+i\gamma}^{\infty+i\gamma} e^{-(\omega-\omega_0)^2 / 4b} \frac{\omega}{a^2 - \omega^2} d\omega \\ &\quad - \frac{i\gamma}{a} \int_{-\infty+i\gamma}^{\infty+i\gamma} e^{-(\omega-\omega_0)^2 / 4b} \frac{a}{a^2 - \omega^2} d\omega, \quad (50) \end{aligned}$$

and where it is assumed that $\nu_0 > \gamma > 0$ and hence $a > 0$. By using the Parseval's relation (47) and the standard transforms (44) through (46), it now follows that

$$\begin{aligned} I &= 2\pi \int_0^{\infty} \sqrt{\frac{b}{\pi}} e^{i\omega_0 t} e^{-bt^2} (-i)^* \cos(at) dt \\ &\quad - \frac{i\gamma}{a} 2\pi \int_0^{\infty} \sqrt{\frac{b}{\pi}} e^{i\omega_0 t} e^{-bt^2} \sin(at) dt. \quad (51) \end{aligned}$$

By rewriting the trigonometric functions using exponentials the integral above can also be written in the more generic form

$$\begin{aligned} I &= \frac{\sqrt{\pi}\alpha}{2\sqrt{\ln 2}} \left(i \int_0^{\infty} e^{-bt^2 + i(\omega_0+a)t} dt \right. \\ &\quad + i \int_0^{\infty} e^{-bt^2 + i(\omega_0-a)t} dt - \frac{\gamma}{a} \int_0^{\infty} e^{-bt^2 + i(\omega_0+a)t} dt \\ &\quad \left. + \frac{\gamma}{a} \int_0^{\infty} e^{-bt^2 + i(\omega_0-a)t} dt \right). \quad (52) \end{aligned}$$

All the integrals above are now in a form where we can substitute and complete the squares inside the exponent to get

$$\begin{aligned} &\int_0^{\infty} e^{-\alpha^2 t^2 / 4 \ln 2 - ct} dt \\ &= \frac{2\sqrt{\ln 2}}{\alpha} e^{c^2 \ln 2 / \alpha^2} \int_0^{\infty} e^{-(t+c\sqrt{\ln 2}/\alpha)^2} dt \\ &= \frac{2\sqrt{\ln 2}}{\alpha} e^{c^2 \ln 2 / \alpha^2} \int_{c\sqrt{\ln 2}/\alpha}^{\infty} e^{-t^2} dt \\ &= \frac{2\sqrt{\ln 2}}{\alpha} e^{c^2 \ln 2 / \alpha^2} \frac{\sqrt{\pi}}{2} \operatorname{erfc}(c\sqrt{\ln 2}/\alpha) \\ &= \frac{\sqrt{\pi \ln 2}}{\alpha} w(ic\sqrt{\ln 2}/\alpha), \quad (53) \end{aligned}$$

where $c = -i(\omega_0 \pm a)$, $\operatorname{erfc}(z)$ is the complementary error function and $w(z) = e^{-z^2} \operatorname{erfc}(-iz)$ the Faddeeva function, see [35, Eq. 7.2.1–7.2.3]. Collecting all the results above, we get finally

$$\begin{aligned} h_{\text{FV}}(\nu) &= \sqrt{\frac{\ln 2}{\pi}} \frac{1}{\alpha} \left(\left(-\frac{\gamma}{a} + i \right) w \left((\nu + a + i\gamma) \frac{\sqrt{\ln 2}}{\alpha} \right) \right. \\ &\quad \left. + \left(\frac{\gamma}{a} + i \right) w \left((\nu - a + i\gamma) \frac{\sqrt{\ln 2}}{\alpha} \right) \right). \quad (54) \end{aligned}$$

B. Uniform convergence of the Voigt profile

We consider the uniform converge of the error term

$$E_{\tilde{\alpha}, \tilde{\gamma}}^{\text{V}}(\tilde{\nu}) = \frac{1}{\sqrt{\pi}} \int_{-\infty}^{\infty} e^{-t^2} \frac{t(2\tilde{\nu} - t)}{\tilde{\gamma}^2 + (\tilde{\nu} - t)^2} dt, \quad (55)$$

where $\tilde{\alpha} = \sqrt{\ln 2}$, $\tilde{\gamma} = (\gamma/\alpha)\sqrt{\ln 2}$ and $\tilde{\nu} = (\nu/\alpha)\sqrt{\ln 2}$ as defined in (23). Assume that $\tilde{\nu} > 0$, let $0 < a < 1$ be a suitable chosen parameter and make the following estimates of $|\tilde{\nu} - t|$ in the respective subintervals

$$\begin{cases} t \leq 0 & \Rightarrow |\tilde{\nu} - t| \geq \tilde{\nu} \\ 0 \leq t \leq a\tilde{\nu} & \Rightarrow |\tilde{\nu} - t| \geq (1-a)\tilde{\nu} \\ a\tilde{\nu} \leq t \leq 2\tilde{\nu} & \Rightarrow |\tilde{\nu} - t| \geq 0 \\ t \geq 2\tilde{\nu} & \Rightarrow |\tilde{\nu} - t| \geq \tilde{\nu}. \end{cases} \quad (56)$$

An error estimate based on (55) is now readily obtained as

$$\begin{aligned} |E_{\tilde{\alpha}, \tilde{\gamma}}^{\text{V}}(\tilde{\nu})| &\leq \frac{1}{\sqrt{\pi}} \int_{-\infty}^0 e^{-t^2} \frac{(-t)(2\tilde{\nu} - t)}{\tilde{\gamma}^2 + \tilde{\nu}^2} dt \\ &\quad + \frac{1}{\sqrt{\pi}} \int_0^{a\tilde{\nu}} e^{-t^2} \frac{t(2\tilde{\nu} - t)}{\tilde{\gamma}^2 + (1-a)^2\tilde{\nu}^2} dt \\ &\quad + \frac{1}{\sqrt{\pi}} \int_{a\tilde{\nu}}^{2\tilde{\nu}} e^{-t^2} \frac{t(2\tilde{\nu} - t)}{\tilde{\gamma}^2} dt \\ &\quad + \frac{1}{\sqrt{\pi}} \int_{2\tilde{\nu}}^{\infty} e^{-t^2} \frac{t(t - 2\tilde{\nu})}{\tilde{\gamma}^2 + \tilde{\nu}^2} dt. \quad (57) \end{aligned}$$

By making the substitution $t \leftrightarrow -t$ in the first integral, and then repeating the whole procedure for negative $\tilde{\nu}$, it is found that

$$\begin{aligned} |E_{\tilde{\alpha}, \tilde{\gamma}}^{\text{V}}(\tilde{\nu})| &\leq \frac{1}{\sqrt{\pi}} \int_0^{\infty} e^{-t^2} \frac{t(2|\tilde{\nu}| + t)}{\tilde{\gamma}^2 + \tilde{\nu}^2} dt \\ &\quad + \frac{1}{\sqrt{\pi}} \int_0^{a|\tilde{\nu}|} e^{-t^2} \frac{t(2|\tilde{\nu}| - t)}{\tilde{\gamma}^2 + (1-a)^2\tilde{\nu}^2} dt \\ &\quad + \frac{1}{\sqrt{\pi}} \int_{a|\tilde{\nu}|}^{2|\tilde{\nu}|} e^{-t^2} \frac{t(2|\tilde{\nu}| - t)}{\tilde{\gamma}^2} dt \\ &\quad + \frac{1}{\sqrt{\pi}} \int_{2|\tilde{\nu}|}^{\infty} e^{-t^2} \frac{t(t - 2|\tilde{\nu}|)}{\tilde{\gamma}^2 + \tilde{\nu}^2} dt. \quad (58) \end{aligned}$$

The right hand side of (58) can now be evaluated by using the following integrals

$$\frac{1}{\sqrt{\pi}} \int_{R_1}^{R_2} e^{-t^2} t dt = \frac{1}{2\sqrt{\pi}} (e^{-R_1^2} - e^{-R_2^2}), \quad (59)$$

and

$$\begin{aligned} &\frac{1}{\sqrt{\pi}} \int_{R_1}^{R_2} e^{-t^2} t^2 dt \\ &= \frac{1}{2\sqrt{\pi}} (R_1 e^{-R_1^2} - R_2 e^{-R_2^2}) + \frac{1}{4} (\operatorname{erf}(R_2) - \operatorname{erf}(R_1)), \quad (60) \end{aligned}$$

and where $\text{erf}(\cdot)$ is the error function [35, Eq. 7.2.1]. By carrying out the integrations above the following upper bound is obtained

$$|E_{\tilde{\alpha}, \tilde{\gamma}}^V(\tilde{\nu})| \leq \frac{1}{\tilde{\gamma}^2 + \tilde{\nu}^2} \left(\frac{1}{2} + \frac{|\tilde{\nu}|}{\sqrt{\pi}} - \frac{1}{4} \text{erf}(2|\tilde{\nu}|) \right) + \frac{1}{\tilde{\gamma}^2 + (1-a)^2 \tilde{\nu}^2} \left(\frac{2|\tilde{\nu}|}{2\sqrt{\pi}} (1 - e^{-a^2 \tilde{\nu}^2}) + \frac{a|\tilde{\nu}|}{2\sqrt{\pi}} e^{-a^2 \tilde{\nu}^2} - \frac{1}{4} \text{erf}(a|\tilde{\nu}|) \right) + \frac{1}{\tilde{\gamma}^2} \left(\frac{(2-a)|\tilde{\nu}|}{2\sqrt{\pi}} e^{-a^2 \tilde{\nu}^2} - \frac{1}{4} (\text{erf}(2|\tilde{\nu}|) - \text{erf}(a|\tilde{\nu}|)) \right). \quad (61)$$

Finally, the bound in (61) can be further relaxed and simplified as

$$|E_{\tilde{\alpha}, \tilde{\gamma}}^V(\tilde{\nu})| \leq \frac{1}{\tilde{\gamma}^2 + \tilde{\nu}^2} \left(\frac{1}{2} + \frac{|\tilde{\nu}|}{\sqrt{\pi}} \right) + \frac{1}{\tilde{\gamma}^2 + (1-a)^2 \tilde{\nu}^2} \frac{(2+a)|\tilde{\nu}|}{2\sqrt{\pi}} + \frac{1}{\tilde{\gamma}^2} \frac{(2-a)|\tilde{\nu}|}{2\sqrt{\pi}} e^{-a^2 \tilde{\nu}^2}. \quad (62)$$

It can readily be seen that the bound in (62) converges to zero uniformly over $\tilde{\nu} \in \mathbb{R}$ as $\tilde{\gamma} \rightarrow \infty$. It can furthermore be seen that (62) is uniformly bounded by an arbitrarily small number $\varepsilon > 0$ for $\tilde{\gamma} > n_1 \sqrt{\ln 2}$ where $n_1 > 0$ is given and $|\tilde{\nu}| > n_3 \sqrt{\ln 2}$ where n_3 is a sufficiently large positive real number.

REFERENCES

- [1] N. N. Filippov, V. P. Ogibalov, and M. V. Tonkov, "Line mixing effect on the pure CO₂ absorption in the 15 μm region," *Journal of Quantitative Spectroscopy & Radiative Transfer*, vol. 72, pp. 315–325, 2002.
- [2] N. N. Filippov and M. V. Tonkov, "Semiclassical analysis of line mixing in the infrared bands of CO and CO₂," *Journal of Quantitative Spectroscopy & Radiative Transfer*, vol. 50, no. 1, pp. 111–125, 1993.
- [3] R. G. Gordon, "Semiclassical theory of spectra and relaxation in molecular gases," *J. Chem. Phys.*, vol. 45, pp. 1649–1655, 1966.
- [4] —, "On the pressure broadening of molecular multiplet spectra," *J. Chem. Phys.*, vol. 46, pp. 448–455, 1967.
- [5] J.-M. Hartmann, C. Boulet, and D. Robert, *Collisional effects on molecular spectra. Laboratory experiments and models, consequences for applications*. Amsterdam: Elsevier, 2008.
- [6] N. Ngo, D. Lisak, H. Tran, and J.-M. Hartmann, "An isolated line-shape model to go beyond the voigt profile in spectroscopic databases and radiative transfer codes," *Journal of Quantitative Spectroscopy & Radiative Transfer*, vol. 129, pp. 89–100, 2013.
- [7] P. W. Rosenkranz, "Shape of the 5 mm oxygen band in the atmosphere," *IEEE Trans. Antennas Propagat.*, vol. 23, no. 4, pp. 498–506, 1975.
- [8] A. Berk and F. Hawes, "Validation of MODTRAN 6 and its line-by-line algorithm," *Journal of Quantitative Spectroscopy & Radiative Transfer*, vol. 203, pp. 542–556, 2017.
- [9] I. E. Gordon, L. S. Rothman, C. Hill, R. V. Kochanov, Y. Tan, P. F. Bernath, M. Birk, V. Boudon, A. Campargue, K. V. Chance, B. J. Drouin, J.-M. Flaud, R. R. Gamache, J. T. Hodges, D. Jacquemart, V. I. Perevalov, A. Perrin, K. P. Shine, M.-A. H. Smith, J. Tennyson, G. C. Toon, H. Tran, V. G. Tyuterev, A. Barbe, A. G. Császár, V. M. Devi, J. J. H. T. Furtenbacher, J.-M. Hartmann, A. Jolly, T. J. Johnson, T. Karman, I. Kleiner, A. A. Kyuberis, J. Loos, O. M. Lyulin, S. T. Massie, S. N. Mikhailenko, N. Moazzen-Ahmadi, H. S. P. Müller, O. V. Naumenko, A. V. Nikitin, O. L. Polyansky, M. Rey, M. Rotger, S. W. Sharpe, K. Sung, E. Starikova, S. A. Tashkun, J. V. Auwera, G. Wagner, J. Wilzewski, P. Wcisło, S. Yu, and E. J. Zak, "The HITRAN2016 molecular spectroscopic database," *Journal of Quantitative Spectroscopy & Radiative Transfer*, vol. 203, pp. 3–69, 2017.
- [10] L. S. Rothman and et al, "The HITRAN molecular spectroscopic database and HAWKS (HITRAN atmospheric workstation): 1996 edition," *Journal of Quantitative Spectroscopy & Radiative Transfer*, vol. 60, no. 5, pp. 665–710, 1998.
- [11] J. Tennyson, P. F. Bernath, A. Campargue, A. G. Császár, L. Daumont, R. R. Gamache, J. T. Hodges, D. Lisak, O. V. Naumenko, L. S. Rothman, H. Tran, N. F. Zobov, J. Buldyreva, C. D. Boone, M. D. D. Vizia, L. Gianfrani, J.-M. Hartmann, R. McPheat, D. Weidmann, J. Murray, N. H. Ngo, and O. L. Polyansky, "Recommended isolated-line profile for representing high-resolution spectroscopic transitions (IUPAC Technical Report)," *Pure Appl. Chem.*, vol. 86, pp. 1931–1943, 2014.
- [12] K. N. Liou, *An introduction to atmospheric radiation*. London, UK: Academic Press, 2002.
- [13] S. M. Abrarov, "The Voigt/complex error function (second version) (<https://www.mathworks.com/matlabcentral/fileexchange/47801-the-voigt-complex-error-function-second-version>), MATLAB Central File Exchange. Retrieved August 26, 2020."
- [14] S. M. Abrarov and B. M. Quine, "Efficient algorithmic implementation of the Voigt/complex error function based on exponential series approximation," *Appl. Math. Comput.*, vol. 218, pp. 1894–1902, 2011.
- [15] F. Schreier, "The Voigt and complex error function: A comparison of computational methods," *Journal of Quantitative Spectroscopy & Radiative Transfer*, vol. 48, no. 5/6, pp. 743–762, 1992.
- [16] G. Kristensson, *Scattering of Electromagnetic Waves by Obstacles*. SciTech Publishing, Edison, NJ, 2016.
- [17] R. G. Newton, *Scattering Theory of Waves and Particles*. New York: Springer-Verlag, 1982.
- [18] N. I. Akhiezer, *The classical moment problem*. Oliver and Boyd, 1965.
- [19] F. Gesztesy and E. Tsekanovskii, "On matrix-valued Herglotz functions," *Math. Nachr.*, vol. 218, no. 1, pp. 61–138, 2000.
- [20] I. S. Kac and M. G. Krein, "R-functions - Analytic functions mapping the upper halfplane into itself," *Am. Math. Soc. Transl.*, vol. 103, no. 2, pp. 1–18, 1974.
- [21] M. Nedic, C. Ehrenborg, Y. Ivanenko, A. Ludvig-Osipov, S. Nordebo, A. Luger, B. L. G. Jonsson, D. Sjöberg, and M. Gustafsson, *Herglotz functions and applications in electromagnetics*. IET, 2019, editor: K. Kobayashi and P. Smith.
- [22] H. M. Nussenzveig, *Causality and dispersion relations*. London: Academic Press, 1972.
- [23] C. F. Bohren and D. R. Huffman, *Absorption and Scattering of Light by Small Particles*. New York: John Wiley & Sons, 1983.
- [24] W. Q. Cai, T. E. Gough, X. J. Gu, N. R. Isenor, and G. Scoles, "Polarizability of CO₂ studied in molecular-beam laser Stark spectroscopy," *Phys. Rev. A*, vol. 36, no. 10, pp. 4722–4727, 1987.
- [25] G. Grynberg, A. Aspect, and C. Fabre, *Introduction to quantum optics*. Cambridge University Press, 2010.
- [26] G. C. Schatz and M. A. Ratner, *Quantum Mechanics in Chemistry*. Mineola, New York: Dover Publications, Inc., 2002.
- [27] J. E. Sipe and J. V. Kranendonk, "Macroscopic electromagnetic theory of resonant dielectrics," *Phys. Rev. A*, vol. 9, no. 5, pp. 1806–1822, 1974.
- [28] F. W. J. Olver, *Asymptotics and special functions*. Natick, Massachusetts: A K Peters, Ltd, 1997.
- [29] C. Sohl, M. Gustafsson, and G. Kristensson, "Physical limitations on broadband scattering by heterogeneous obstacles," *J. Phys. A: Math. Theor.*, vol. 40, pp. 11 165–11 182, 2007.
- [30] A. Bernland, A. Luger, and M. Gustafsson, "Sum rules and constraints on passive systems," *Journal of Physics A: Mathematical and Theoretical*, vol. 44, no. 14, pp. 145 205–, 2011. [Online]. Available: <http://dx.doi.org/10.1088/1751-8113/44/14/145205>
- [31] C. F. Bohren and E. E. Clothiaux, *Fundamentals of Atmospheric Radiation*. Weinheim: WILEY-VCH Verlag GmbH & Co. KGaA, 2006.
- [32] G. W. Petty, *A First Course in Atmospheric Radiation*. Madison, Wisconsin: Sundog Publishing, 2006.
- [33] S. J. Blundell and K. M. Blundell, *Concepts in thermal physics*. New York: Oxford University Press Inc., 2010.
- [34] M. Šimečková, D. Jacquemart, L. S. Rothman, R. R. Gamache, and A. Goldman, "Einstein A-coefficients and statistical weights for molecular absorption transitions in the HITRAN database," *Journal of Quantitative Spectroscopy & Radiative Transfer*, vol. 98, pp. 130–155, 2006.
- [35] F. W. J. Olver, D. W. Lozier, R. F. Boisvert, and C. W. Clark, *NIST Handbook of mathematical functions*. New York: Cambridge University Press, 2010.